Journal of Electronics and Information Science (2023)
Clausius Scientific Press, Canada

DOI: 10.23977/jeis.2023.080502
ISSN 2371-9524 Vol. 8 Num. 5

Acceleration of Radiation Analysis Using an Arbitrary High Order Difference Method with Non-uniform Mesh

Jun Li*, Qun Zhang, Peng Jiang, Aote Zhang

Department of Electromagnetism, INTESIM, Dalian, Liaoning, 116000, China
jun.li@intesim.com
**Corresponding author*

Keywords: Non-uniform mesh, Finite Difference Time Domain, Local time step

Abstract: For the analysis of irregular structures, an arbitrary high-order finite difference time-domain local time step based on non-uniform grids is proposed. Comparison with Finite Difference Time Domain, this new method based on non-uniform mesh weak the limit of the time-step size. For the new method allows different grids to interate with different time-step sizes. In order to perform fast and accurate electromagnetic analysis on the responsible problem, it is necessary to use multi-scale grids to segment the target. Using appropriate time steps to solve electromagnetic fields on different grids, achieving accurate and fast analysis of problems. Due to breaking through the limitation of grid size on time step size, the computational workload of the work is reduced. In addition, multi-time steps are implemented by local time step and an arbitrary high order is added to this work to promise the accuracy of computation. This work has great value in practical application engineering.

1. Introduction

It has been proved that finite-difference-time-domain (FDTD) [1][2][3] method is an effective approach that can predict the field of electromagnetic interaction problem. The conventional finite difference time domain (FDTD) method is usually limited by computer memory and running time. In order to break these restrictions, we usually use sub-grid technology to reduce the size of the object. This technology decreases the amount of unknowns so that achieves greater performance. However it is usually difficult to guarantee the stability of this technology. Therefore, we choose non-uniform mesh technology to replace sub-grid technology. The stability of non-uniform mesh technology is similar to conventional FDTD(uniform-grid technology)[4] [5]. Non-uniform mesh technology and uniform mesh technology must satisfy the Courant-Friedrich-Levy (CFL) condition [6] when we use them. Consequently, the minimum size of cell determines the time-step size of the whole calculation. This leads the technology inefficient for the problems when involves fine scale dimensions, such as enclosure with slots [7]. In order to simulate the electromagnetic characteristics of thin slit accurately, the space increment must be smaller than the wavelength. Fine elements reduce the time-step size, which leads to an expensive computation in the conventional FDTD way.

To weaken the limit of CFL on the time-step size of FDTD, an arbitrary high order difference method with non-uniform mesh on the time-step size is proposed. This new method adopts non-

uniform mesh that would reduce the amount of calculation. Besides we use local time step between non-uniform mesh. In addition, the new approach is an arbitrary high order difference method, therefore the accuracy of the method can be adjusted by the order.

2. Theory and formulation

2.1. An Arbitrary High Order FDTD

Maxwell's partial differential equations is transformed as below

$$\frac{\partial \boldsymbol{U}}{\partial t}=\begin{bmatrix} 0 & 0 & 0 & 0 & -\frac{1}{\varepsilon}\frac{\partial}{\partial z} & \frac{1}{\varepsilon}\frac{\partial}{\partial y} \\ 0 & 0 & 0 & \frac{1}{\varepsilon}\frac{\partial}{\partial z} & 0 & -\frac{1}{\varepsilon}\frac{\partial}{\partial x} \\ 0 & 0 & 0 & -\frac{1}{\varepsilon}\frac{\partial}{\partial y} & \frac{1}{\varepsilon}\frac{\partial}{\partial x} & 0 \\ 0 & \frac{1}{\mu}\frac{\partial}{\partial z} & -\frac{1}{\mu}\frac{\partial}{\partial y} & 0 & 0 & 0 \\ -\frac{1}{\mu}\frac{\partial}{\partial z} & 0 & \frac{1}{\mu}\frac{\partial}{\partial x} & 0 & 0 & 0 \\ \frac{1}{\mu}\frac{\partial}{\partial y} & -\frac{1}{\mu}\frac{\partial}{\partial x} & 0 & 0 & 0 & 0 \end{bmatrix}\begin{bmatrix} E_x \\ E_y \\ E_z \\ H_x \\ H_y \\ H_z \end{bmatrix}=Q\boldsymbol{U} \tag{1}$$

where $\boldsymbol{U}=\begin{bmatrix}\boldsymbol{E}\\ \boldsymbol{H}\end{bmatrix}$ and

$$Q=\begin{bmatrix} 0 & 0 & 0 & 0 & -\frac{1}{\varepsilon}\frac{\partial}{\partial z} & \frac{1}{\varepsilon}\frac{\partial}{\partial y} \\ 0 & 0 & 0 & \frac{1}{\varepsilon}\frac{\partial}{\partial z} & 0 & -\frac{1}{\varepsilon}\frac{\partial}{\partial x} \\ 0 & 0 & 0 & -\frac{1}{\varepsilon}\frac{\partial}{\partial y} & \frac{1}{\varepsilon}\frac{\partial}{\partial x} & 0 \\ 0 & \frac{1}{\mu}\frac{\partial}{\partial z} & -\frac{1}{\mu}\frac{\partial}{\partial y} & 0 & 0 & 0 \\ -\frac{1}{\mu}\frac{\partial}{\partial z} & 0 & \frac{1}{\mu}\frac{\partial}{\partial x} & 0 & 0 & 0 \\ \frac{1}{\mu}\frac{\partial}{\partial y} & -\frac{1}{\mu}\frac{\partial}{\partial x} & 0 & 0 & 0 & 0 \end{bmatrix} \tag{2}$$

Repeat the time derivative of (3), we obtain time derivative of each order of the electric and magnetic fields.

$$\frac{\partial \boldsymbol{U}}{\partial t}=Qt \tag{3}$$

$$\boldsymbol{U}\left(t+\Delta t\right)=\boldsymbol{U}\left(t\right)+\sum_{l=1}^{m}\frac{\Delta t^{l}}{l!}\left(\frac{\partial \boldsymbol{U}\left(t\right)}{\partial t}\right)^{l} \tag{4}$$

According to taylor series expansion (4), we can get $\boldsymbol{U}\left(t+\Delta t\right)$. By iterating over time, we can the value of the electric and magnetic fields at any time point.

In order to simulate target in infinite space, we apply Berenger Perfectly Matched Layer (PML)[8] to absorb the electromagnetic wave in finite space(select PEC to cut off).

The electric and magnetic fields iterate in PML through the below steps.

The first step: $\boldsymbol{H}\rightarrow\boldsymbol{D}$, take D_x for example.

$$\frac{\partial H_z}{\partial y}-\frac{\partial H_y}{\partial z}=\kappa_y\frac{\partial D_x}{\partial t}+\frac{\sigma_y}{\varepsilon_0}D_x \tag{5}$$

Then the iteration of ADER in PML is as

$$\frac{\partial D_x}{\partial t}=\frac{1}{\kappa_y}\left(\frac{\partial H_z}{\partial y}-\frac{\partial H_y}{\partial z}-\frac{\sigma_y}{\varepsilon_0}D_x\right) \tag{6}$$

The other components of $\boldsymbol{D}$ are obtained by the cycle substitution of x, y and z.

The second step: $\boldsymbol{D}\rightarrow\boldsymbol{E}$, take E_x for example.

$$\frac{\partial E_x}{\partial t}=\frac{1}{\varepsilon_1\kappa_z}\left(\kappa_x\frac{\partial D_x}{\partial t}+\frac{\sigma_x}{\varepsilon_0}D_x-\frac{\varepsilon_1}{\varepsilon_0}\sigma_z E_x\right) \tag{7}$$

The third step: $\boldsymbol{E}\rightarrow\boldsymbol{B}$, take B_x for example.

$$\frac{\partial B_x}{\partial t}=-\frac{1}{\kappa_y}\left(\frac{\partial E_z}{\partial y}-\frac{\partial E_y}{\partial z}+\frac{1}{\varepsilon_0}\sigma_y B_x\right) \tag{8}$$

The fourth step: $\boldsymbol{B}\rightarrow\boldsymbol{H}$, take H_x for example.

$$\frac{\partial H_x}{\partial t}=\frac{1}{\mu_1\kappa_z}\left(\kappa_x\frac{\partial B_x}{\partial t}+\frac{\sigma_x}{\varepsilon_0}B_x-\frac{\mu_1}{\varepsilon_0}\sigma_z H_x\right) \tag{9}$$

After the four steps, $\frac{\partial H_y}{\partial t}$, $\frac{\partial H_z}{\partial t}$, $\frac{\partial D_x}{\partial t}$ are known. Then we can get the second-order time derivative of (6) as:

$$\frac{\partial^2 D_x}{\partial t^2}=\frac{1}{\kappa_y}\left(\frac{\partial^2 H_z}{\partial t\partial y}-\frac{\partial^2 H_y}{\partial t\partial z}-\frac{\sigma_y}{\varepsilon_0}\frac{\partial D_x}{\partial t}\right) \tag{10}$$

Repeat above step, we obtain x, y and z components of $\frac{\partial^2\boldsymbol{E}}{\partial t^2}$, $\frac{\partial^2\boldsymbol{B}}{\partial t^2}$ and $\frac{\partial^2\boldsymbol{H}}{\partial t^2}$. Therefore, we can get any order time derivative of $\boldsymbol{D}$, $\boldsymbol{E}$, $\boldsymbol{B}$ and $\boldsymbol{H}$. Through taylor series expansion (4), the next time step of $\boldsymbol{D}$, $\boldsymbol{E}$, $\boldsymbol{B}$ and $\boldsymbol{H}$ are achieved.

2.2. Non-uniform mesh

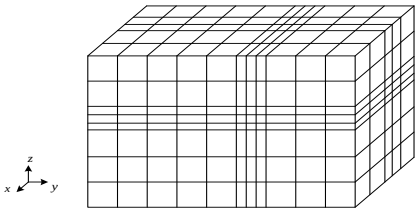

Figure 1: Sketch of the non-uniform mesh.

In this work, the electric fields define at the midpoint of the edge of the Yee cell and magnetic fields define at the center of the face of the Yee cell.

In order to simulation efficiently, more than two kinds of mesh sizes are used in computation (in Fig. 1). According to requirement of the target geometry and electromagnetic parameters, different sizes of gird are used in different regions.

For convenience, H' (the red point in Fig. 2) is added in non-uniform grid computing.

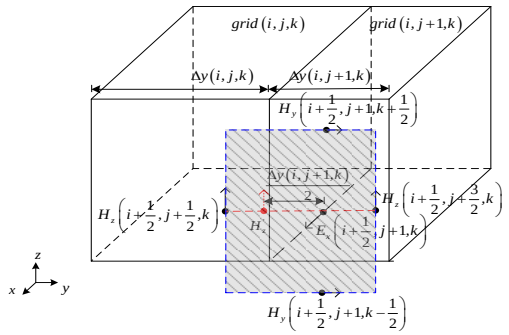

Figure 2: The electric field of non-uniform Yee cell.

As is shown in Fig. 2, Yee cells are non-uniform in the Y direction. Δy of Yee cell $(i,j+1,k)$ and (i,j,k) are different. In solving the first derivative of time at $E_x\left(i+\frac{1}{2},j+1,k\right)$, $H_z^{'}$ is proposed as intermediate transition variable. The position of $H_z^{'}$ is between $H_z\left(i+\frac{1}{2},j+\frac{1}{2},k\right)$ and $H_z\left(i+\frac{1}{2},i+\frac{3}{2},k\right)$ and the distance of $H_z^{'}$ and $E_x\left(i+\frac{1}{2},j+1,k\right)$ is $\frac{\Delta y(i,j+1,k)}{2}$. According to Maxwell's partial differential equations, we get:

$$\begin{aligned} H_z^{'} &= \frac{\left[H_z\left(i+\frac{1}{2},j+\frac{3}{2},k\right)-H_z\left(i+\frac{1}{2},j+\frac{1}{2},k\right)\right]}{\left[\Delta y(i,j,k)+\Delta y(i,j+1,k)\right]/2} \\ &\cdot\left[\Delta y(i,j,k)/2-\Delta y(i,j+1,k)/2\right]+H_z\left(i+\frac{1}{2},j+\frac{1}{2},k\right) \end{aligned} \tag{11}$$

Take (12) into the first line equation of (1), then

$$\begin{aligned} \frac{\partial E_x^n\left(i+\frac{1}{2},j+1,k\right)}{\partial t} &= \frac{H_z^n\left(i+\frac{1}{2},j+\frac{3}{2},k\right)-H_z^{'}}{\bar{\varepsilon}_{E_x}\left(i+\frac{1}{2},j+1,k\right)\cdot\Delta y(i,j+1,k)} \\ &-\frac{H_y^n\left(i+\frac{1}{2},j+1,k+\frac{1}{2}\right)-H_y^n\left(i+\frac{1}{2},j+1,k-\frac{1}{2}\right)}{\varepsilon\left(i+\frac{1}{2},j+1,k\right)\cdot\Delta z} \end{aligned} \tag{12}$$

Where c is dielectric parameters of point $\left(i+\frac{1}{2},j,k\right)$. it is at the junction of four grids, they are $(i,j,k),(i,j+1,k),(i,j,k-1)$ and $(i,j+1,k-1)$ respectively. We make a simple approximation to the value of $\bar{\varepsilon}_{E_x}\left(i+\frac{1}{2},j,k\right)$.

$$\begin{aligned} &\bar{\varepsilon}_{E_x}\left(i+\frac{1}{2},j,k\right) \\ &=\frac{\varepsilon(i,j,k)+\varepsilon(i,j+1,k)+\varepsilon(i,j,k-1)+\varepsilon(i,j+1,k-1)}{4} \end{aligned} \tag{13}$$

According to (13), the iterative formula derivation of non-uniform grid in X direction and Z direction can be obtained.

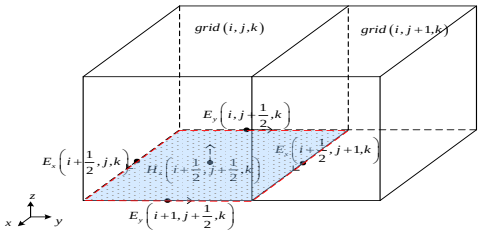

Figure 3: The magnetic field of non-uniform Yee cell.

As shown in Fig. 3, the solution of magnetic field of non-uniform grid and uniform grid are identical. Therefore, the iterative formula do not change.

2.3. Local Time Step

Local time step is used to accelerate ADER on non-uniform mesh. In simulation, we use different time steps (Δt) on mesh of different sizes.

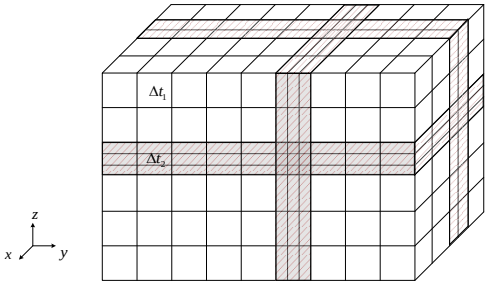

Figure 4: Local time step of non-uniform Yee cells.

As is shown in Fig. 4, there are more than two time steps on the non-uniform Yee cell. The time-step size of most Yee cells is Δt_1 and the time-step size of blue Yee cells in z direction is Δt_2 ($\Delta t_2 = \Delta t_1 / i, i = 2,3\cdots$). Different Yee cells employ different time steps in computation. Large time-step size is adopted for large space cell size and little time-step size is adopted for little space cell size. This new method is more efficient than the FDTD method and the ADER method.

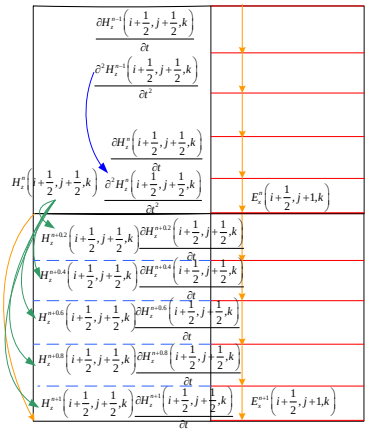

(From top to bottom, it indicates different time periods of the same grid. From left to right, it means different grids at the same time).

Figure 5: Illustration of the local time step algorithm in space showing the space-time elements

As is shown in Fig. 5, it is assumed that one time step of coarse grid is equal to five time steps of fine grid. Therefore, the coarse grid is iterated by one step and the fine grid is iterated by five steps. The iteration of this method is completed in the following steps:

1) As the blue arrow shown in Fig 5, through (15) and (16), $\frac{\partial H_z^n\left(i+\frac{1}{2},j+\frac{1}{2},k\right)}{\partial t}$ and $\frac{\partial^2 H_z^n\left(i+\frac{1}{2},j+\frac{1}{2},k\right)}{\partial t^2}$ is obtained by interpolation from $\frac{\partial H_z^{n-1}\left(i+\frac{1}{2},j+\frac{1}{2},k\right)}{\partial t}$, $\frac{\partial H_z^{n-1}\left(i+\frac{1}{2},j+\frac{1}{2},k\right)}{\partial t}$ and $\frac{\partial^3 H_z^{n-1}\left(i+\frac{1}{2},j+\frac{1}{2},k\right)}{\partial t^3}$.

$$\frac{\partial H^n}{\partial t}=\frac{\partial H^{n-1}}{\partial t}+\sum_{l=1}^{m}\frac{\Delta t^l}{l!}\frac{\partial^{l+1}H^{n-1}}{\partial t^{l+1}} \tag{14}$$

$$\frac{\partial^2 H^n}{\partial t^2}=\frac{\partial^2 H^{n-1}}{\partial t^2}+\sum_{l=1}^{m}\frac{\Delta t^l}{l!}\frac{\partial^{l+2}H^{n-1}}{\partial t^{l+2}} \tag{15}$$

We apply $m=2$ in the operation of (15) and $m=1$ in operation of (16).

After this operation, we can iterate electric field and magnetic field through (1).

2) As the yellow arrow shown in fig 5, we iterate the electric field at position $\left(i+\frac{1}{2},j+1,k\right)$.

3) We iterate the electric and magnetic field at position $\left(i+\frac{1}{2},j+\frac{1}{2},k\right)$.

4) As the green arrow shown in fig 5, the value of magnetic field at time n+0.2 is obtained by interpolation at time n through (17), (18) and (19).

$$H^{n+0.2}=H^n+\sum_{l=1}^{m}\frac{\Delta t^l}{l!}\frac{\partial^l H^n}{\partial t^l} \tag{16}$$

$$\frac{\partial H^{n+0.2}}{\partial t}=\frac{\partial H^n}{\partial t}+\sum_{l=1}^{m}\frac{\Delta t^l}{l!}\frac{\partial^{l+1}H^n}{\partial t^{l+1}} \tag{17}$$

$$\frac{\partial^2 H^{n+0.2}}{\partial t^2}=\frac{\partial^2 H^n}{\partial t^2}+\sum_{l=1}^{m}\frac{\Delta t^l}{l!}\frac{\partial^{l+2}H^n}{\partial t^{l+2}} \tag{18}$$

Loop the same way, we can obtain $H_z^{n+0.4}\left(i+\frac{1}{2},j+\frac{1}{2},k\right)$, $\frac{\partial H_z^{n+0.4}\left(i+\frac{1}{2},j+\frac{1}{2},k\right)}{\partial t}$, $\frac{\partial H_z^{n+0.4}\left(i+\frac{1}{2},j+\frac{1}{2},k\right)}{\partial t}$,… $H_z^{n+1}\left(i+\frac{1}{2},j+\frac{1}{2},k\right)$, $\frac{\partial H_z^{n+1}\left(i+\frac{1}{2},j+\frac{1}{2},k\right)}{\partial t}$, $\frac{\partial^2 H_z^{n+1}\left(i+\frac{1}{2},j+\frac{1}{2},k\right)}{\partial t^2}$.

Through the above steps, the iteration of electric field and magnetic field of adjacent Yee grids and different grids can be realized.

2.4. Numerical Stability

LTS-ADER method, the ADER method and the FDTD method are conditionally stable. The maximum time-step size in this method is determined by spatial increments Δx, Δy and Δz. The

time-step sizes of LTS-ADER with non-uniform mesh are large than or equal to the time-step size of other method with uniform mesh. It is very useful to realize different time-step sizes in different space cell size with the LTS-ADER method.

3. Numerical results

The CPU has Intel core Q9500 and 8GB memory. The environment is based on the Fortran MPI.

In order to demonstrate the accuracy and efficiency of the ADER-LTS, we give a numerical example. Fig. 6 schematically shows an enclosure with three different slots.

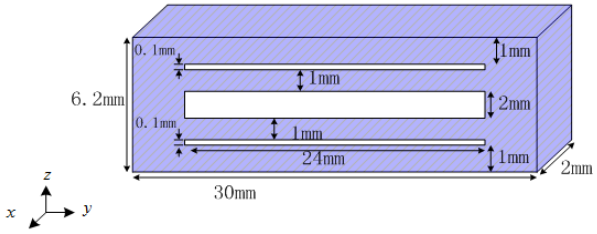

Figure 6: Enclosure with three different slots.

In Fig. 6, the length, width, and height of the enclosure are 30, 2, 6.2mm respectively. There are three slots on the front side of the enclosure. The size for the two thin slots is 24mm*0.1mm and for the wide slot, it is 24mm*2mm. An excitation source of Gauss pulse is located on the front of the enclosure. The Incident angle of θ=90^0 and φ=0^0. An excitation source of Gauss pulse is located on the front of the enclosure. The center frequency of incident pulse is 150GHz and the pulse width is 2.4ns. The grid size of FDTD is $dx = 0.2$ mm, $dy = 0.2$ mm and $dz = 0.02$ mm. ADER-LTS has two grid sizes. The fine size is $dx = 0.2$ mm, $dy = 0.2$ mm, $dz = 0.02$ mm and the rough size is $dx = 0.2$ mm, $dy = 0.2$ mm, $dz = 0.2$ mm. The fine gird is operated at the two thin slots, the other part uses the rough grid to compute. The time step size for the FDTD method is $\Delta t = 0.7/c\sqrt{1/0.0002^2 + 1/0.0002^2 + 1/0.00002^2} = 0.462\times10^{-13}$ s. There are two time step sizes for the ADER-LTS method. The time step size of fine gird is 0.462×10^{-13} s and the time step size of the rough gird is 2.772×10^{-13} s.

Table 1: Result of Fdtd and Ader-Lts

	Time consuming	Totall cell
ADER-LTS	2281.23s	64*204*94
FDTD	21484.75s	64*204*850

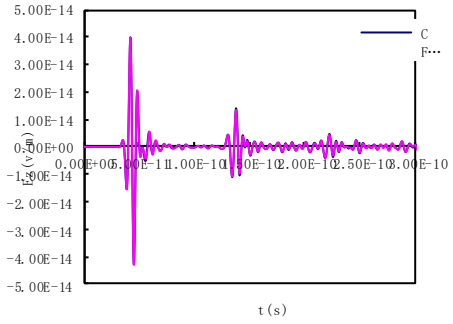

Figure 7: Comparison of the electric field component E_z calculated by FDTD and ADER-LTS methods.

In Fig 7, it shows the high precision of ADER-LTS. From the data of TABLE 1, ADER-LTS shows high computational efficiency.

The third example is a dual-band bandpass filter (Fig 8), which is design for WLAN. The central frequencies of the two passband are designed at 2.35GHz and 5.37GHz. The dielectric constant and the thickness of the substrate is $\varepsilon_r = 9.8$ and $h = 1.524$ mm. It is realized by using a 50ohm input and output transmission line.

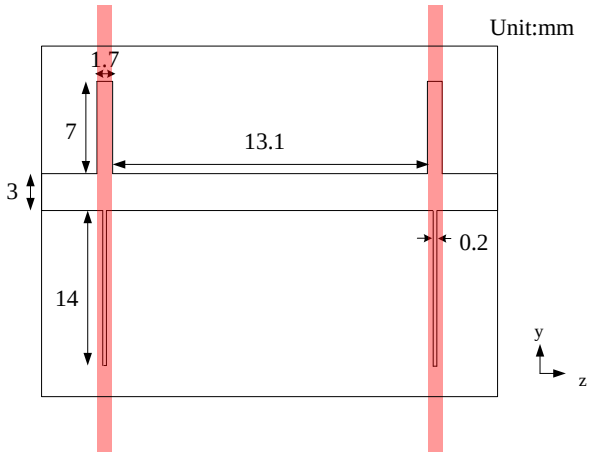

Figure 8: Circuit configuration of dual-band bandpass filter.

The grid size of FDTD is $dx = 0.254$ mm, $dy = 0.25$ mm and $dz = 0.025$ mm. ADER-LTS has two grid sizes. The fine size is $dx = 0.254$ mm, $dy = 0.25$ mm, $dz = 0.025$ mm (the red zone in fig 7) and the rough size is $dx = 0.254$ mm, $dy = 0.25$ mm, $dz = 0.25$ mm. The time step size of fine gird is 0.826×10^{-13} s and the time step size of the rough gird is 4.956×10^{-13} s.

Table 2: Result of Fdtd and Ader-Lts

	Time consuming	Totall cell
ADER-LTS	127.61h	60*173*316
FDTD	399.52h	60*173*1740

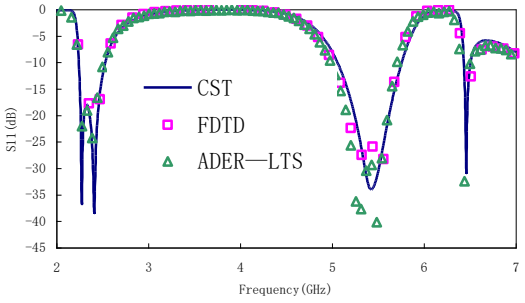

Figure 9: Comparison of FDTD simulated, ADER-LTS simulated and CST simulated results.

In Fig 9, it shows the high precision of ADER-LTS. TABLE 2 shows the high computational efficiency of ADER-LTS.

4. Conclusion

This paper introduces a 3-D ADER-LTS for solving Maxwell's equation. With non-uniform mesh, we use different time-step sizes in different spatial discretizations. The ADER-LTS method

not only can be used in the analysis of thin slots and some antenna, but also can be useful in other electromagnetic problems where both fine and electrically large structures are used.

Acknowledgements

The authors acknowledge the Technology Talent Entrepreneurship Support Program：“Multi-physical Field Strong Weak Coupling CAE Software Platform of” (No: 2020RC01).

References

[1] Gedney D S, “An anisotropic perfectly matched layer-absorbing medium for the truncation of FDTD lattices,” IEEE Transactions on Antennas & Propagation, vol. 44, no. 12, pp. 1630-1639, 2002.
[2] Namiki T, “3-D ADI-FDTD method-unconditionally stable time-domain algorithm for solving full vector Maxwell's equations,” IEEE Transactions on Microwave Theory & Techniques, vol.48, no. 10, pp. 1743-1748, 2000.
[3] Jin N, Rahmat-Samii Y, “Parallel particle swarm optimization and finite- difference time-domain (PSO/FDTD) algorithm for multiband and wide-band patch antenna designs,” IEEE Transactions on Antennas & Propagation, vol. 53, no. 11, pp. 3459-3468, 2005.
[4] Shi Shouyuan, “Analysis of diffractive optical elements using a nonuniform finite-difference time-domain method,” Optical Engineering, vol. 40, no. 4, pp. 503-510, 2001.
[5] Kermani M H, Ramahi O M, “The complementary derivatives method: a second-order accurate interpolation scheme for non-uniform grid in FDTD simulation,” IEEE Microwave & Wireless Components Letters, vol. 16, no. 2, pp. 60-62, 2006.
[6] Namiki T, “A new FDTD algorithm based on alternating-direction implicit method,” IEEE Transactions on Microwave Theory and Techniques, vol. 47, no. 10, pp. 2003-2007, 1999.
[7] Chen J, Wang J, “A Three-Dimensional HIE-PSTD Scheme for Simulation of Thin Slots,” IEEE Transactions on Electromagnetic Compatibility, vol. 55, no. 6, pp. 1239-1249, 2013.
[8] Berenger J.-P, “Perfectly matched layer for the FDTD solution of wave-structure interaction problems,” Antennas and Propagation, IEEE Transactions on, 1996.